Development of a hydrodynamic model for a subtropical reservoir: Salto Grande, Uruguay

R. Rodríguez[1], S. Delgado[1], M. Fossati[1], P. Santoro[1]
[1] Universidad de la República, Montevideo, Uruguay.
psantoro@fing.edu.uy

***Abstract* – The objective of this work is to characterize the hydrodynamics and transport time scales of the main hydroelectric generation reservoir in Uruguay based on a numerical modelling approach. The work is based on the analysis of numerical results from a hydrodynamic model implemented for the Salto Grande reservoir, using the TELEMAC-MASCARET Modelling System (TMS).**

A 2D depth-averaged approach is followed. The model is calibrated and validated using data of surface elevation at several stations along the river-reservoir system. The obtained results show good agreement with the measured data, representing satisfactorily the main features of the Salto Grande dynamics.

A simulation with realistic forcings during several years allows us to analyse the circulation in the river-reservoir system, and the estimation of the transport time scales based on numerical experiments with a passive tracer. The effect of the wind forcing is also analysed.

Keywords: reservoir, circulation, transport time scales.

I. INTRODUCTION

Hydropower reservoirs are semi-lentic water bodies that, in addition to power generation, have other uses e.g., water supply, fishing and recreation. Typically, the increase in the water residence time combined with the increasing process of anthropical eutrophication favours the occurrence of phytoplanktonic blooms. These events have negative consequences on the ecosystem (affecting both its physical-chemical properties and the biota) and interfere with human activities. This work aims to contribute to a better management of the hydropower reservoirs water quality by developing numerical tools that help to understand the system dynamics and allow to predict its future behaviour.

II. STUDY AREA

The Salto Grande Hydroelectric Complex (CHSG) is located on the Uruguay River (31°16'28.7"S, 57°56'21.0"W, kilometer 342.6), upstream from the cities of Concordia (Argentina) and Salto (Uruguay), see Figure 1. The Uruguay River basin up to the CHSG covers an area of approximately 244,000 km^2. The immediate basin is located between the city of Paso de los Libres and the Salto Grande dam and covers an approximate area of 47,200 km^2. The Salto Grande reservoir is an artificial lake with multiple purposes, including energy production, drinking water and recreational activities. It is a reservoir with a dendritic morphology, composed of a single main entrance, the Uruguay River (mean flow rate of 4,400m^3/s), and multiple lateral tributaries, of which the most relevant in terms of flow contributions are the Arapey River (mean flow rate of 65 m^3/s) and the Mocoreta River (mean flow rate of 43 m^3/s). Table 1 shows the main characteristics of the reservoir [1]. In the last three decades, multiple scientific works have addressed the phenomenon of phytoplankton blooms in the Salto Grande reservoir, giving an account of the water quality problems in this water body [2][3][4][5][6].

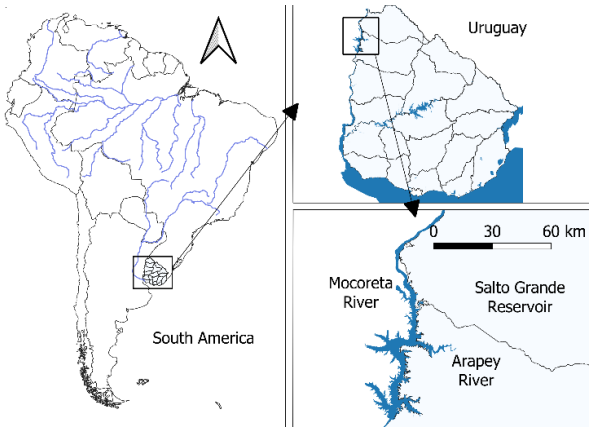

Figure 1. Location of the study area, Salto Grande reservoir.

Table I Main characteristics of Salto Grande reservoir.

Nominal water level (m)	35
Area (km^2)	783
Perimeter (km)	1,190
Volume (hm^3)	5,500
Reservoir length (km)	140
Mean width (km)	5.4
Maximal width (km)	9

III. METHODOLOGY

A. *Numerical model implementation*

The numerical model TELEMAC-MASCARET (www.opentelemac.org) is used, in particular its two-dimensional hydrodynamic module TELEMAC-2D [7]. It solves the depth-averaged free-surface flow equations (Saint-Venant equations), using the finite element method on unstructured grids of triangular elements.

1) *Mesh and bathymetry*

The computational domain is shown in Figure 2. It includes the Salto Grande reservoir and several kilometers of its main

tributary (Uruguay River) up to Paso de los Libres (PL) where boundary conditions are imposed. Some islands in the reservoir were included as land area. The mesh consists of approximately 28,000 nodes and 49,500 elements with dimensions varying from 250 m up to 125 m in refined zones. The bathymetry is provided by the Joint Technical Commission of Salto Grande (CTM-SG), for the area between the dam and Paso de la Cruz (PC in Figure 2). Between PC and PL there is not available bathymetric information, so a linear profile was assumed. The slope is computed based on the available bathymetric information in the last part of the river up to PC.

There is a relatively dense bathymetry (more than 115,000 points in an area of 684 km^2), obtained from more than 400 transversal profiles separated between 500 and 1,000 meters (with spatial resolution of approximately 10 meters), and longitudinal profiles for the main channel and the main tributaries. The bathymetry data is provided by CTM-SG validated to the year 2019 and covers the reservoir region from the dam to approximately 10 kilometres upstream of Monte Caseros (MC in Figure 2).

Several interpolation methods are tested to generate the model bathymetry. The deterministic methods implemented in ArcGIS are used. Although good results are obtained locally (e.g., with Radial Basis Functions), when observing the results globally (i.e.: interpolation between cross-sectional profiles) discontinuities are observed that deviated from what is expected at a natural margin of a river channel. Adding this qualitative criterion, the best results are obtained using the inverse of the distance squared considering the closest 4 points located in different quadrants. Between MC and PL a bottom slope of 1.68x10^{-4} is imposed, value computed from the slope of the last fluvial region with available data.

2) Boundary conditions

The open boundaries of the domain correspond to the dam (output flow) and all the reservoir tributaries (input flows). There are both measured and unmeasured flows in the reservoir. The measured flows are supplied by CTM-SG at Paso de los Libres (PL), Paso de la Cruz (PC), Arapey grande (AG), Arapey chico (AC) and Dam (DA) stations (see locations in Figure 2). On the other hand, there are unmeasured inflows corresponding to the following tributaries: Itapebí Grande (IG), Itapebí Chico (IC), Mocoreta (MO), Mandisovi Chico (MCh), Mandisovi Grande (MG) and Gualeguaycito (G); see Figure 2. The CTM-SG also provided a theoretical total hydrological inflow to the reservoir, computed from a mass balance. The unmeasured flows were computed by distributing the difference between the theoretical total hydrological contribution flow and the sum of the measured inflow flows, proportional to the basin area of each tributary.

At the free surface the effect of the wind was considered. Wind data was obtained from the ECMWF ERA5 reanalysis product [8].

The model is then forced by inflows and outflows as well as the surface wind stress. The boundary conditions in the open boundaries are the free surface elevation and flow discharged at the Dam, using a Thompson boundary condition [9], and flow rates (measured or estimated) in the other open boundaries.

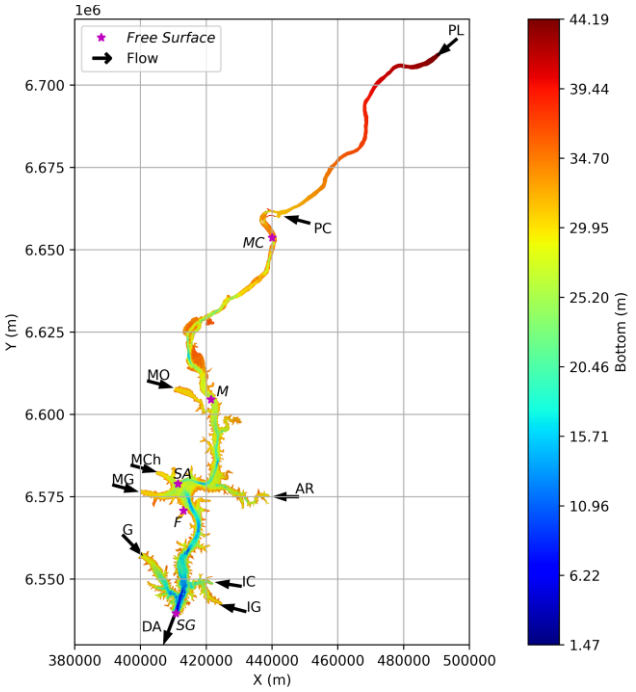

Figure 2. Simulation domain, mesh and bathymetry. Open boundary conditions are indicated as well.

3) Model calibration and verification

There are six free surface elevation gauge stations: Monte Caseros (MC), Mocoreta (MO), Federación (F), Santa Ana (SA), Salto Grande (SG) and Dam (DA). Unfortunately, there is not available water velocity data for model calibration.

The model is then calibrated based on the free surface elevation data. The bottom friction and wind drag coefficients are selected as calibration parameters.

The calibration period is 2019/01/10 until 2020/04/30 (15 months approx., period called window 2). The calibration parameters include the Manning roughness coefficient (n) for which the values 0.020, 0.024, 0.025, 0.026 and 0.030 s/m$^{1/3}$ are tested. On the other hand, the following values are considered for the COEFFICIENT OF WIND INFLUENCE: 1.0x10^{-6}, 1.25x10^{-6}, 1.5x10^{-6}, and 2.0x10^{-6}. The mean absolute error (MAE), root mean square error (RMSE), and BIAS are used to assess the model performance. The model is then validated for the free surface elevation at the MC, M, SA, F, and SG stations, for two time windows: from 2018/2/28 to 2018/7/20 (approx. 5 months, period called window 1), and from 2020/5/27 to 2020/10/21 (approx. 5 months, period called window 3).

The time step used for these simulations is 5 s. The Smagorinsky formulation is used for turbulence closure with a base value of eddy diffusivity of 1x10^{-6} m^2/s and tracer diffusivity of 1 m^2/s.

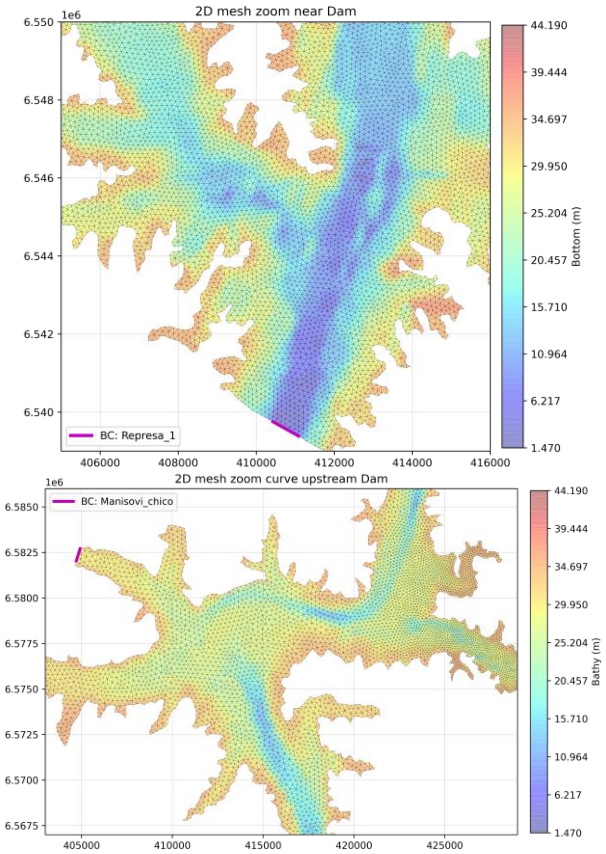

Figure 3. Detail of the simulation mesh and bathymetry in the lower (upper panel) and middle (lower panel) reaches of the reservoir.

B. *Hydrodynamic characterization*

In order to characterize the reservoir hydrodynamic the mean, 10 and 90 percentile maps are computed based on the model results for the simulated period (2017/02-2020/10). The water flux through the entrance of the Gualeguaycito arm is also calculated (see Figure 2). Finally, the influence of the wind on these results is analysed.

To estimate the transport time scales in this work we propose to adapt two local parameters: the exponential flushing time (flushing time - t_{FT}) and the flushing lag time (flushing lag - t_{FL}). They come from an Eulerian methodology which calculation method is adopted from [10]. Initially, a concentration $C_0 = 1$ of a passive tracer is imposed within the domain and a concentration value $C^* = 0$ is assigned to the water flow entering through open boundaries. The time taken for the concentration to reach a threshold value C_1 (arbitrarily set as 95% of C_0) is called flushing lag time and is considered to be the beginning of an exponential decrease in concentration at the observed domain point. The t_{FT} is defined as the "local e-flushing time" and corresponds to the time taken from t_{FL} for the concentration of the passive tracer to reach a value of $1/e\text{^}C_0$. Both parameters are called local as they are computed for each node of the mesh.

Considering the underlying hypothesis of this methodology it is better suited to analyse steady scenarios. Three scenarios without wind are tested for this work, combining different surface elevations and incoming flowrates at PL: 1) (scenario e3) low level at the dam (percentile 10: SG=32.96 m) and high flowrates (percentile 90: DA=11,586 m^3/s; IG=57 m^3/s; IC=31 m^3/s; AR=469 m^3/s; PC=1,112 m^3/s; PL=9,528 m^3/s; MO=274 m^3/s; MCh=36 m^3/s; MG=46 m^3/s; G=33 m^3/s); 2) (scenario e6) average surface elevation (mean value: SG=34.31 m) and average flowrates (mean value: DA=5,389 m^3/s; IG=25 m^3/s; IC=15 m^3/s; AR=224 m^3/s; PC=395 m^3/s; PL=4,563 m^3/s; MO=113 m^3/s; MCh=17 m^3/s; MG=21 m^3/s; G=16 m^3/s); 3) (scenario e11) high surface elevation (percentile 90: SG=35.32 m) and high flowrates (percentile 90).

Then the wind influence is tested by simulating eight scenarios with average free surface elevation and incoming flowrates, and a constant wind of 10 m/s blowing from eight different cardinal directions.

IV. RESULTS AND DISCUSSION

A. *Model calibration and verification*

The simulated free surface elevation is not very sensitive to the Manning roughness coefficient for the stations located at the lower part of the reservoir (SG, F, and SA), showing variations in the RMSE and MAE of the order from millimetre to centimetre. On the other hand, stations M and MC, which show a transitional and fluvial behaviour respectively, present a greater sensitivity with RMSE and MAE variations of centimetres to decimetre. Regarding the wind drag coefficient, the model presented little sensitivity for all stations in the calibration period, with variations between simulations of the order of a millimetre.

Figure 4 shows qualitatively the results obtained for station F and MC with n = 0.025 $s/m^{1/3}$ and $C_D = 1.0x10^{-6}$ for the calibration period, together with the measured inflows. Table II presents quantitatively the results of the evaluation of the predictions for the calibration and validation periods. The model reproduces reasonably well the water surface elevation at both stations which have different behaviours.

Table II Model performance statistics at stations F and MC for the calibration (Window 2) and validation periods (Windows 1 and 3).

Station *F*	**Window 1**	**Window 2**	**Window 3**
RMSE (m)	0.110	0.138	0.122
MAE (m)	0.101	0.127	0.118
BIAS (m)	-0.099	-0.108	-0.118
Station *MC*	**Window 1**	**Window 2**	**Window 3**
RMSE (m)	0.149	0.223	0.290
MAE (m)	0.116	0.175	0.263
BIAS (m)	0.039	-0.007	0.254

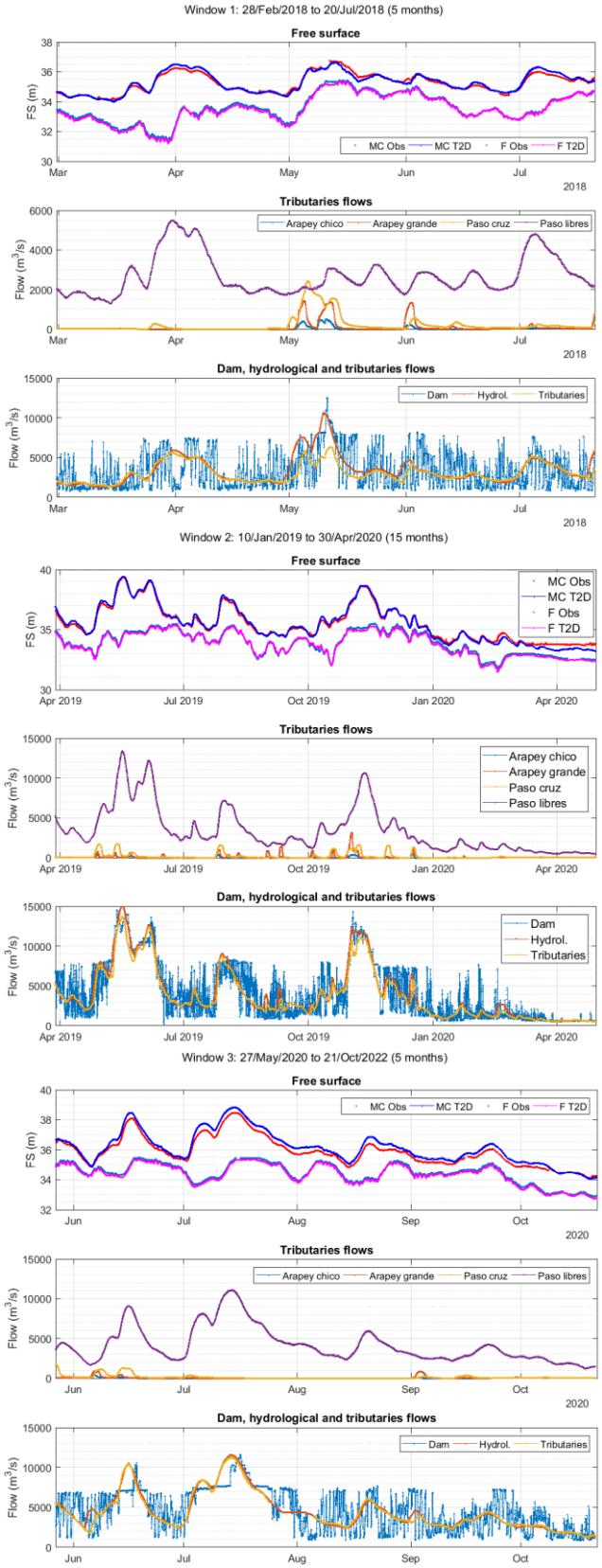

Figure 4. Observed (Obs) and simulated free surface elevations (T2D) for station F and MC (see Figure 1), and measured inflows. Calibration (Window 2) and validation periods (Windows 1 and 3) are shown.

B. *Water circulation*

The mean velocity field (Figure 5) for the simulated period shows a clear difference between the central zone and the reservoir arms, as expected. The mean intensities in the central zone show values around 10 cm/s, while in the arms are one order of magnitude lower. At the Gualeguaycito arm (Figure 5 upper panel) it is interesting to note the circulation patterns showing higher intensities near the coast. This is usually related to the wind effect on the shallower areas and have been reported in other study cases like [11].

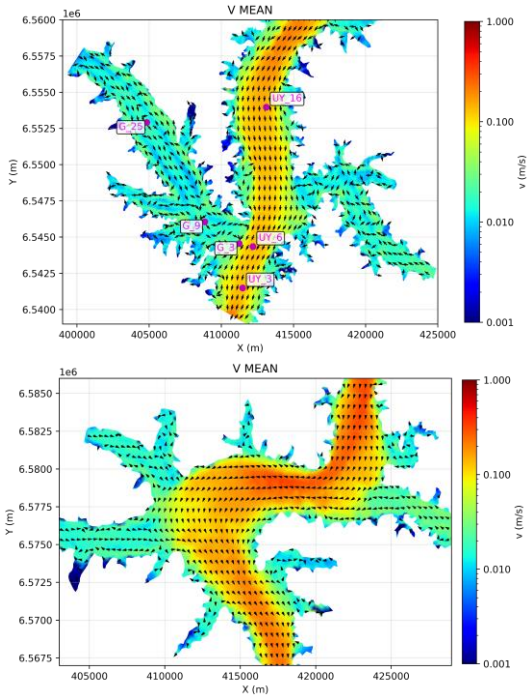

Figure 5. Mean velocity field for the period 2017/02-2020/10 at the lower and middle reaches of the reservoir.

Figures 6 and 7 show the 90 and 10 percentile maps for the simulated period at the lower reservoir reach, while Figure 8 shows a boxplot of the intensity time series at the stations indicated in Figure 5. At the central zone the effect of the flood events is more noticeable showing currents intensities close to 1 m/s.

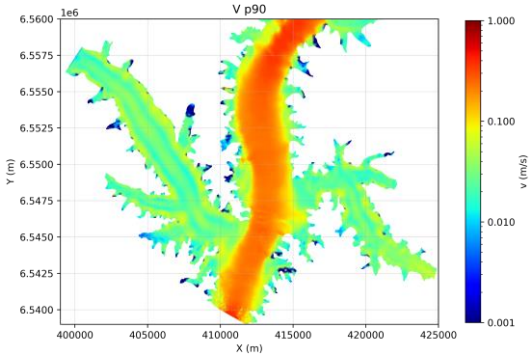

Figure 6. Percentile 90 of current intensities for the simulated period 2017/02-2020/10.

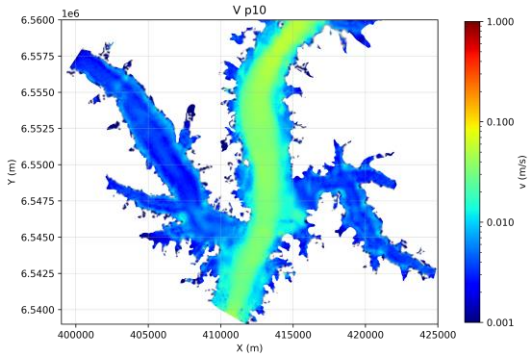

Figure 7. Percentile 10 of current intensities for the simulated period 2017/02-2020/10.

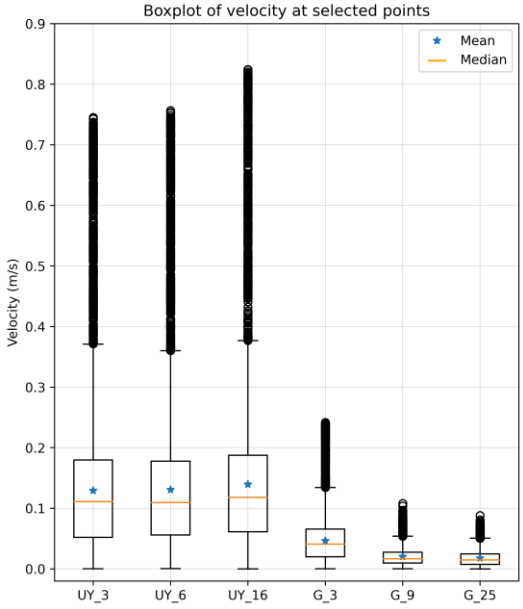

Figure 8. Boxplot of current intensities at several stations at the reservoir lower reach (see Figure 5).

The influence of the wind forcing is relevant specially in the reservoir arms. Figure 9 shows the mean velocity field obtained without including the wind forcing and the difference with the mean current field with wind (presented in Figure 5). As expected the differences are noticeable in shallower areas; specially the Gualeguaycito arm shows a significant change in its circulation patterns and intensities.

C. Transport time scales

Figure 10 shows an example of the tracer concentration evolution in the three scenarios without wind at one station located in the central zone (UY_6, see Figure 5) and another in the Gualeguaycito arm (G_25). The thresholds for the flushing lag and local flushing time are indicated as well. It can be seen that the exponential decay assumption underlying the methodology is reasonable in these steady scenarios.

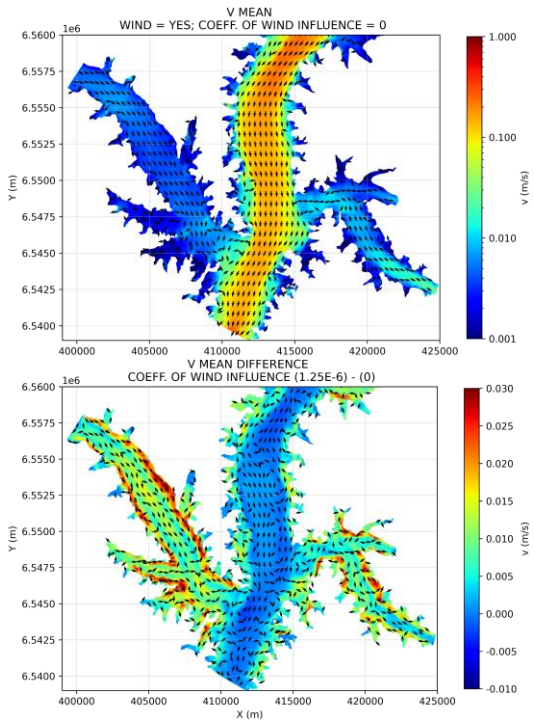

Figure 9. Mean velocity field without wind forcing (upper panel) and its difference with the mean velocity field shown in Figure 5 (lower panel).

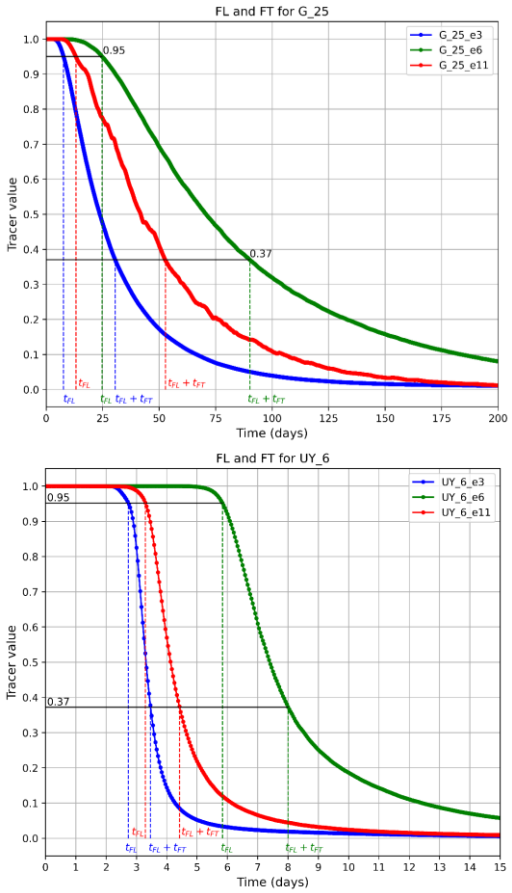

Figure 10. Example of tracer concentration evolution at stations G_25 and UY_6 for the scenarios e3, e6 and e11.

Figures 11 and 12 show the flushing lag and local flushing time maps for the three scenarios without wind forcing and different combinations of water level and inflow rates. The flushing lag results, which give an idea of the arrival time, show lower values in the central zone where the advection is dominant, as well as in the arms close to the open boundaries with imposed inflows. As expected, higher inflow rates and lower water level tends to decrease the flushing time and vice versa. For the mean scenario the flushing time in the central zone is in the order of a few days, while in the Gualeguaycito arm for example can be up to two months.

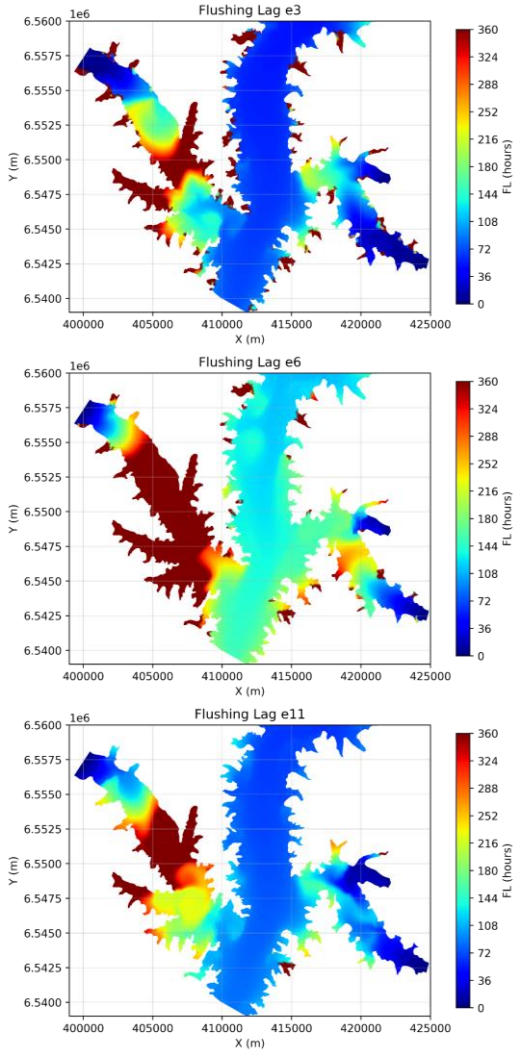

Figure 11. Maps of flushing lag (FL) for the scenarios with low water level and high inflow (e3); mean water level and inflow rate (e6); and high water level and inflow rates (e11).

Figures 13 and 14 show the flushing lag and local flushing time maps for the scenarios with different wind directions. Only four directions are shown (SW, SE, NE, and NW). As it was seen previously in the mean velocity fields, the wind forcing is relevant in the reservoir arms, while the central zone does not show significant changes.

The flushing lag maps clearly show how the fluvial inflow is advected towards the wind direction in the Gualeguaycito arm. When the wind blows cross to the arm (SW and NE directions) the flow is concentrated on the south and north coast respectively. Wind blowing along the arm and towards the reservoir tends to enhance the advection (NW wind) and the opposite when it blows towards the coast (SE wind).

The flushing time maps (Figure 14) shows that wind directions along the arm direction tend to increase the water exchange with the central zone leading to lower transport time scales. On the other hand winds blowing with transversal direction to the arm show much higher transport time scales and an enhanced shear flow at the arm entrance.

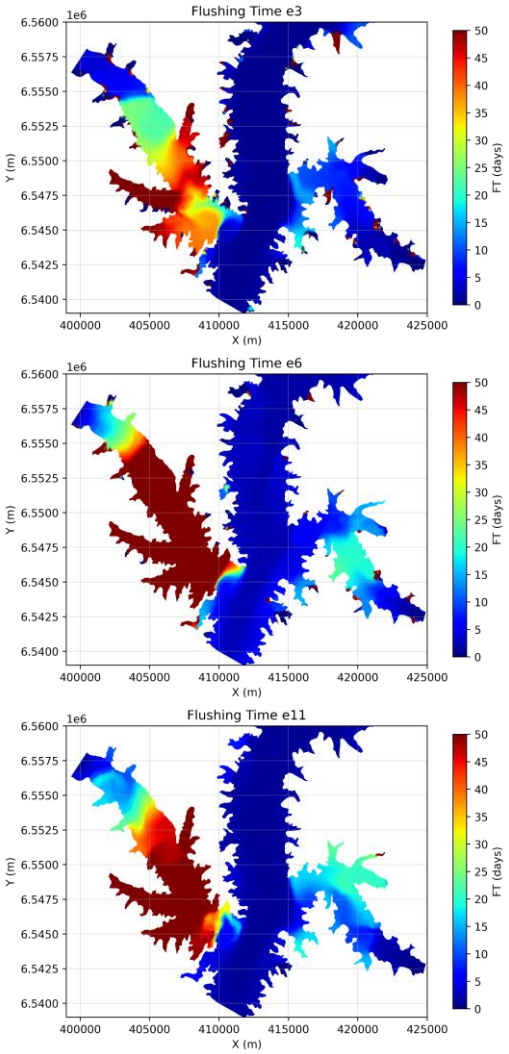

Figure 12. Maps of flushing time (FT) for the scenarios with low water level and high inflow (e3); mean water level and inflow rate (e6); and high water level and inflow rates (e11).

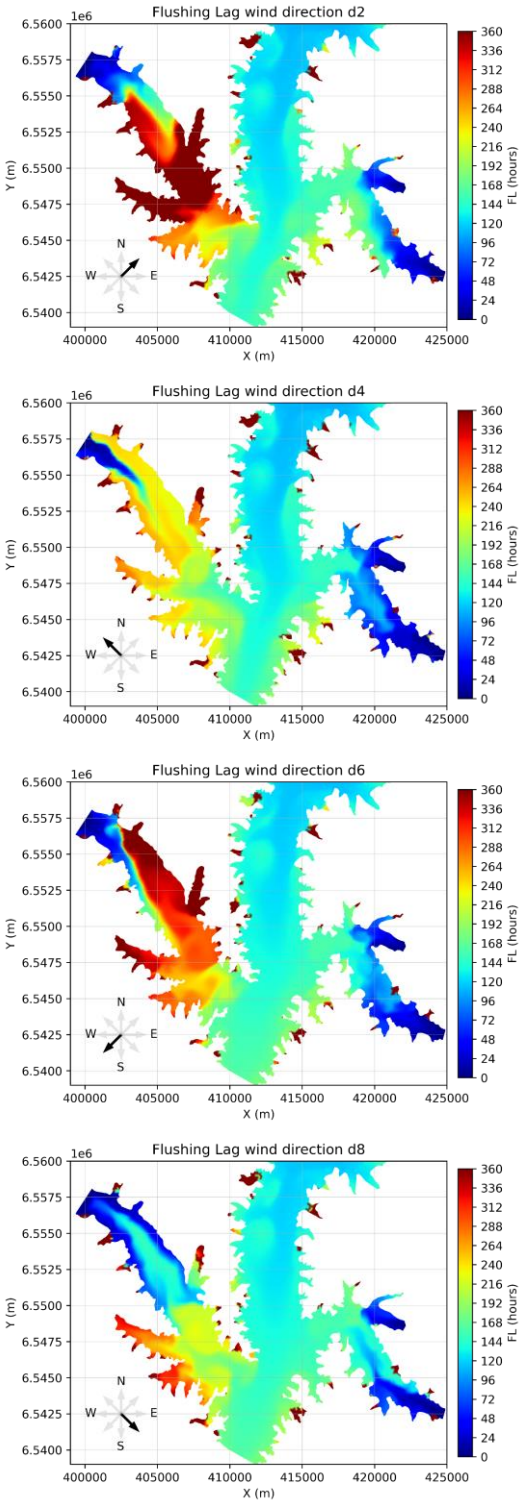

Figure 13. Maps of flushing lag (FL) for the scenarios with mean level and inflow and four different wind directions.

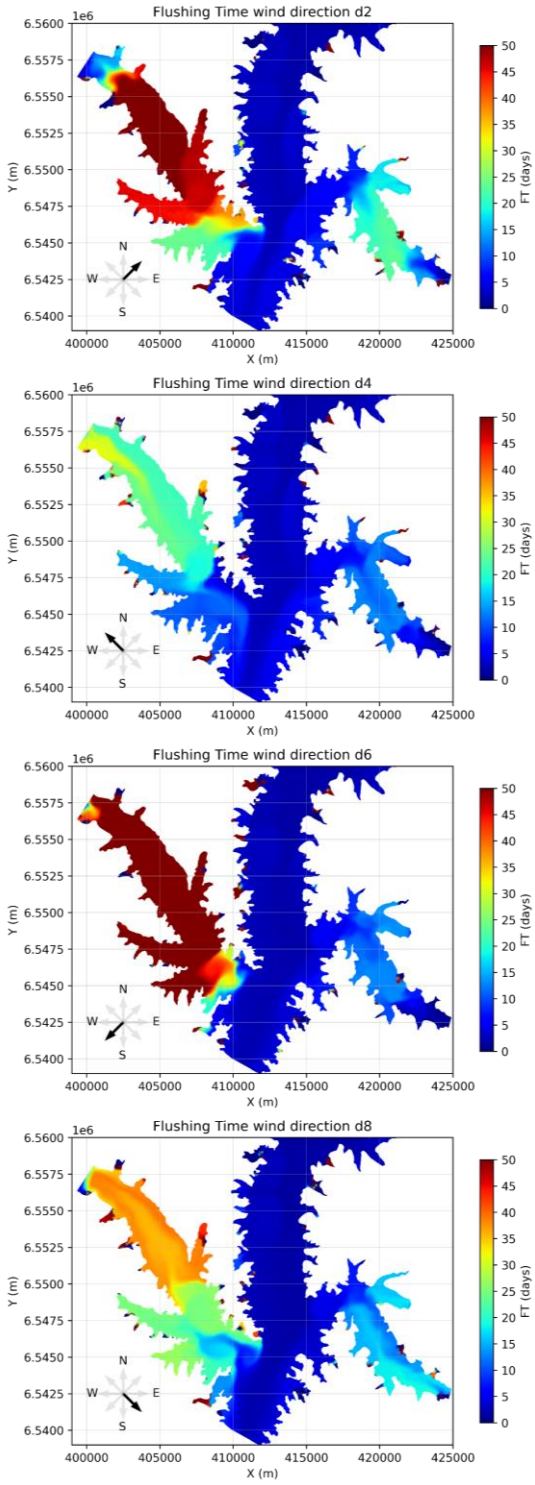

Figure 14. Maps of local e-flushing time (FT) for the scenarios with mean level and inflow and four different wind directions.

V. CONCLUSIONS AND FUTURE WORK

In this work a depth averaged hydrodynamic model is implemented for the Salto Grande hydropower reservoir. The model is able to reproduce adequately the water surface elevation behaviour in different zones of the reservoir with fluvial and transitional regimes.

The circulation in the reservoir is analysed based on the results of a 4 years simulation with realistic forcings. The velocity fields show a clear difference between the reservoir central zone and arms. The wind influence is assessed through numerical experiments and shows to be relevant on the arms circulation.

Numerical experiments with a passive tracer allow us to analyse the transport time scales in the reservoir under idealized steady scenarios. The results show lower transport time scales in the central zone where the advection is dominant. In the reservoir arms the wind again showed to be relevant, and its direction in relation to the arm axis shown may enhance or decrease the transport time scales. This is relevant considering that these arms are the most promised in terms of water quality problems.

Ongoing studies include the evaluation of other techniques to estimate the transport time scales with the numerical model (lagrangian approaches, non-steady scenarios), and a better characterization of the circulation patterns using other methods like empirical orthogonal functions.

ACKNOWLEDGEMENT

This work has been carried out within the framework of the ANII-FMV 2019 research project “Numerical tools to support water quality management in hydropower reservoirs”.

The authors would like to thank the scientific committee, which improved the earlier version of this article.

REFERENCES

[1] CTM-SG, 2018. Memoria Anual de Gestión. https://www.saltogrande.org/memoria_gestion/Memoria_Gestion_2018.pdf

[2] L.E. Berón, (1990). Features of the limnological behavior of Salto Grande’s reservoir (Argentina-Uruguay). Ecological Modelling, 52, 87-102.

[3] R. Quirós, and L. Luchini (2005). Características Limnológicas del Embalse de Salto Grande, III: Fitoplancton y su Relación con Parámetros Ambientales. Natura Neotropicalis, 1(13), 49-66.

[4] I. O’Farrell, F. Bordet, and G. Chaparro (2012). Bloom forming cyanobacterial complexes cooccurring in a subtropical large reservoir: validation of dominant eco-strategies. Hydrobiologia 698 (1), 175-190.

[5] F. Bordet, MS. Fontanarrosa, I. O’Farrell, (2017). Influence of light and mixing regime on bloom-forming phytoplankton in a subtropical reservoir. River Research and Applications, 33 (8), 1315-1326.

[6] A. Drozd, P. de Tezanos Pinto, V. Cañal Fernández, M. Bazzalo, F. Bordet, and G. Ibáñez (2019). Hyperspectral remote sensing monitoring of cyanobacteria blooms in a large South American reservoir: high- and medium-spatial resolution satellite algorithm simulation. Marine and Freshwater Research, 71, 593-605.

[7] J.-M. Hervouet (2007). Hydrodynamics of Free Surface Flows: Modelling with the finite element method. John Wiley & Sons, Ltd.

[8] H. Hersbach, et al. (2020). The ERA5 global reanalysis. Q J R Meteorol Soc. 146, 1999– 2049. https://doi.org/10.1002/qj.3803

[9] J.-M. Hervouet, C. Denis and E. David (2011). Revisiting the Thompson boundary conditions. Proceedings of the XVIIIth Telemac & Mascaret User Club 2011, 142-147.

[10] A. Jouon, P. Douillet, S. Ouillon, and P. Fraunié (2006). Calculations of hydrodynamic time parameters in a semi-opened coastal zone using a 3D hydrodynamic model. Continental Shelf Research, 26, 1395-1415.

[11] O. Boutron, O. Bertrand, A. Fiandrino, P. Höhener, A. Sandoz, Y. Chérain, E. Coulet, and P. Chauvelon, (2015). An unstructured numerical model to study wind-driven circulation patterns in a managed coastal mediterranean wetland: The Vaccarès lagoon system. Water (Switzerland), 7 (11), 5986-6016. https://doi.org/10.3390/w7115986